Supplementary Material (ESI) for Journal of Materials Chemistry

Synthesis of Silver Nano- Fir-Twigs and Application to Single Molecules Detection

Salah Habouti, Claus-Henning Solterbeck and Mohammed Es-Souni*

[*] Prof. M. Es-Souni
Institute for Materials & Surface Technology, University of Applied Sciences
Grenzstrasse 3, 24149 Kiel, Germany
e-mail: me@fh-kiel.de

Summary

We process silver nanostructures via electrodeposition into porous aluminium oxide templates. The degree of pore ordering determines the morphology of the silver nanostructure from smooth to branched nanowires. Nanostructures reminiscent of fir-twigs form in templates with large and low-ordered pores. We demonstrate the usefulness of these nano-fir-twigs as SERS substrates using a 10^{-15} M R6G dye solution. The enhancement factor of 10^{11} obtained should allow single molecules to be detected.

1. Introduction

Nanomaterials with controlled shape and dimension are in the focus of materials research as they may display unusual chemical and physical properties that could be used in various applications.[1-3] For instance, the interaction of light with metallic nanostructures excites plasmon resonance on their surfaces, and this phenomenon may be exploited for a variety of applications including photonics, biosensing and molecular detection.[1-2,4-7] Routes to the synthesis of nanomaterials are multiple, though mostly versatile ones are based on soft chemistry.[8,9] For the fabrication of self-assembled 1D-nanostructures with controllable sizes, aspect ratios and gaps template aided synthesis using porous membranes is also widely used. The filling of the channels is achieved either by soaking the membrane in appropriate precursor solutions, or chemicals, or by electrodeposition.[10] The latter is probably best suited for the fabrication of nanowires of various metals.[10-12]

The outstanding optical properties of metallic nanostructures arise from the coupling between plasmons of adjacent, self-assembled or patterned nanoparticles. For particular gap lengths this coupling leads to the formation of nanoscale “hot spots” in which the electromagnetic field is enhanced by several orders of magnitude.[1-2, 4,6,13] This phenomenon has been used for more than a decade for the detection of trace amounts of molecules and dyes using Raman scattering[14,15] (Surface Enhanced Raman Scattering (SERS) in the following). SERS enhancement factors (EF) may attain so huge a value on one “hot-spot” of self-assembled metallic nanostructures that a single molecule may be detected.[4] Yet this requires a tedious search for the one hot-spot that would lead to appropriate signal enhancement. For a colloidal suspension of noble metal particles, or self-assembled monolayers of them, a distribution of SERS EF are normally found within $3x10^4$ to $4x10^{10}$ (the latter is

required for few to single molecule detection).[13] Thus it appears that the development of cost-effective substrates that ensure reproducibly enhanced signals is a prerequisite for a wider application of SERS beyond fundamental studies.

In recent work, the potential of TiO_2-Ag_xO nanocomposites for fabricating SERS substrates with controlled Ag-particle size, shape and gap using a simple irradiation process after nanocomposite fabrication has been shown.[16] SERS EF as high as $4.5x10^6$ were reproducibly obtained on these robust substrates over large probe areas. In the present work we extended our efforts to the synthesis of specific Ag-nanostructures, in particular those reminiscent to fir twigs, and we show that SERS EF higher than the maximum value of $4x10^{10}$ reported for the hottest spots of self-assembled Ag-nanoparticles can be obtained on rhodamine 6G dye molecules resulting in substantial signal enhancement from 10^{-15} molar solutions (1fM) .[13]

2. Experimental Details.

The templates employed were Commercial AAO filters (Whatman Anodisc® filters SPI, US) and self-made AAO templates. The latter were fabricated starting from 0.25 mm thick high-purity Al foils (99.999%, Goodfellow, UK). The foils were first degreased in acetone for 20 min and subsequently annealed in flowing nitrogen for 5 hours at 500 °C. Prior to anodization the Al-sheets were electrochemically polished in a solution of 75 vol% perchloric acid and in ethanol. Anodization was performed in an aqueous 0.3M solution of oxalic acid at 40V and 17°C following the two-step anodization method[17]. The sacrificial layer formed in the first step was removed by soaking for 24h in an aqueous solution of 5 wt% phosphoric acid and 8 wt% chromic acid at 70 °C. Well ordered pores are obtained in the second anodization step where an anodization time of 6h resulted in a membrane thickness of 30 μm. The remaining aluminium was dissolved in a $CuCl_2$ /HCl solution. Further processing included pore opening on the back-side, and this was achieved via a 45 minutes soaking in an

aqueous solution of 5% phosphoric acid at 30 °C. Subsequently a 60 nm thick film was sputtered on one side of the membrane followed by Cu-plating to ensure membrane stability and good electrical contact. Ag-electrodeposition was performed in a lab-built electrochemical cell with Ag/AgCl as Reference electrode and a broad Pt-sheet as counter electrode. The template was mounted in the cell with its open side facing the electrolyte. Before deposition the membrane together with the cell were washed with deionized water before the silver electrolyte was filled in. The silver electrolyte was an aqueous solution of $AgNO_3$ (Roth, Germany), the pH of which was adjusted to 2 by adding glacial acetic acid (Roth, Germany). During electrodeposition the voltage was maintained at a constant value of -200 $mV_{Ag/AgCl}$. The current was recorded during deposition. Deposition into the pores was performed in an area of approximately 28 mm^2 over a thickness of 35 µm for the commercial AAO and 30 µm for the self-made AAO membrane. For comparison, thin film Al_2O_3 thin films were processed via sol-gel and spin-coating on silicon substrates. The precursor solution was prepared from Al-sec-butoxide (Sigma Aldrich, Germany), acetylacetone (Roth, Germany) and ethanol as solvent. Microstructure was investigated by means of high resolution scanning electron microscopy (Zeiss Ulra Plus, Germany) and X-ray diffraction (X'Pert Pro, PanAnalytical, Holland). For SERS measurements 10^{-3}M aqueous solution of Rhodamine 6G (Sigma Aldrich, Germany) and Methyl orange (Roth, Germany) were prepared and diluted successively to 10^{-15}M and 10^{-11}M, respectively. The substrates were immersed in the corresponding solution and maintained for 12h. After drying Raman measurements were performed on a Raman microscope (Senterra, Brucker, Germany) using a 532 nm laser radiation and laser power of 0.2mW. The integration time was 10s for Rhodamine 6G and 1s for Methyl orange. The Raman signal was recorded using a CCD camera.

3. Results and discussion

The Ag-nano-fir-twigs (Ag-NFIT) were processed via electrodeposition in porous anodic aluminum oxide (AAO) templates. Electrolyte and deposition parameters were optimized in order to achieve deposition into the pores. Although there exists a plethora of work on template synthesis of nanomaterials, reports on successful electrodeposition of Ag-nanowires (Ag-NW) into the pores are scarce.[18] Ag-NW and other nanostructures are usually synthesized using other methods.[19-22] Ag was electrodeposited into two different AAO templates with different pore ordering and pore size; one purchased (designated hereafter as CAAO) and the other self-made (HAAO). CAAO templates have irregular pore morphology and ordering with a mean pore size of 200 nm (Fig. 1a), and their cross-section shows branched pore channels. The number of pores per unit area was estimated to be close to $10^9/cm^2$. The HAAO templates (see experimental section for a description of their processing method) have hexagonally ordered pores with a mean pore diameter of 70 nm and continuous single pore channels (Fig. 1c). In this case the number of pores per unit area was estimated to be $1.1x10^{10}/cm^2$.

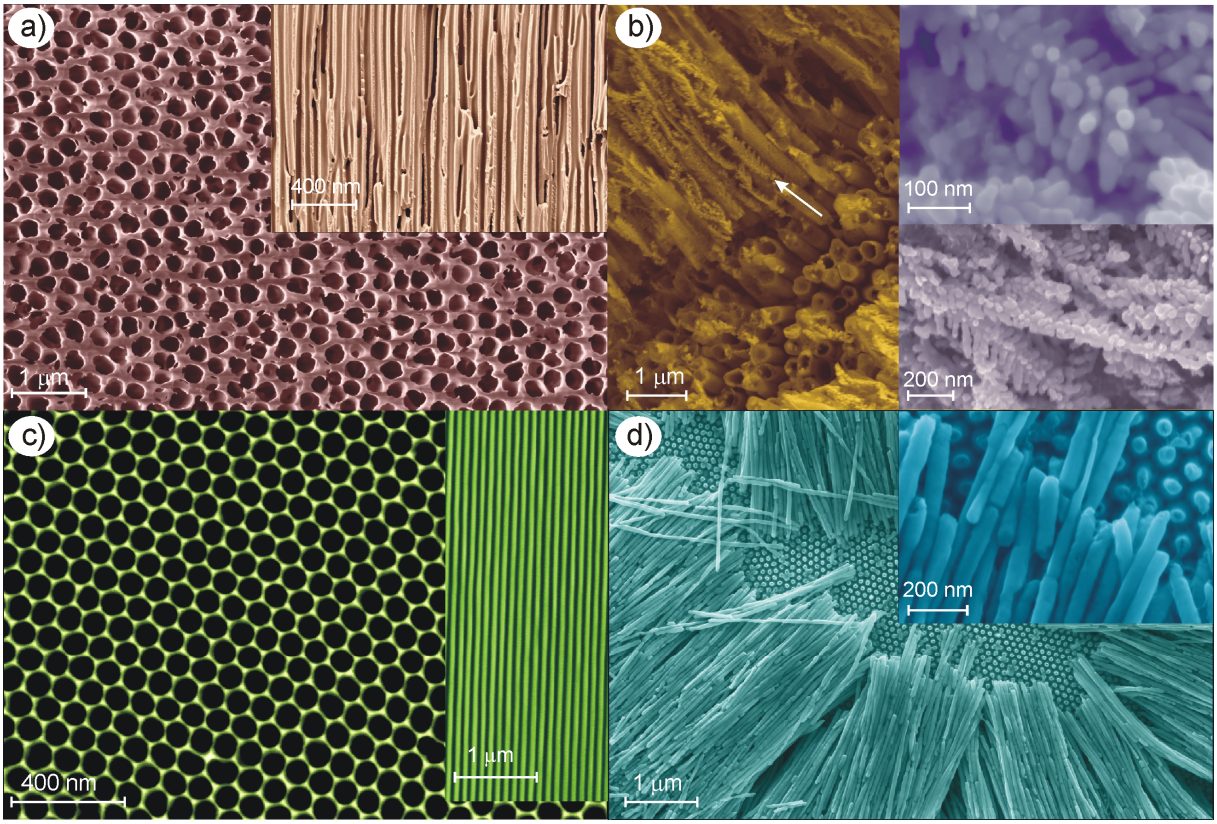

Fig. 1 High-resolution Secondary electron micrographs of a) morphology of commercial anodized aluminum oxide (CAAO) membranes showing the irregular pore shape and ordering; the inset shows a cross-section of the CAAO membrane where pore branching can be seen. b) Shows silver nano-fir-twigs (Ag-NFIT) obtained by electrodeposition in the CAAO template; the arrow point to Ag-NFIT in a cross-section of the filled CAAO template. The inset shows a high magnification micrograph of the Ag-NFIT demonstrating the 3D character of the nanostructure. c) Self-made AAO membranes with hexagonal, well ordered pores and homogeneous pore size (70 nm) and distribution. The inset shows a cross section of the membrane with its continuous single channel morphology. d) Shows bundles of Ag-nanowires obtained by electrodeposition in the self-made AAO membrane after membrane dissolution

The kinetics in both membranes is different as may be seen from the current-time curves (see supporting information, Fig. 1s). Both curves show transients characteristic for parabolic growth. However, fast growth at slightly higher currents dominates in the CAAO template and the nanowires reach the membrane surface quite rapidly after 20 minutes deposition time (steep increase in the current-time

curve). In the HAAO template the deposition current remains almost constant over a larger period of time after a short transient, denoting a smooth electrolyte-solid interface. The specific morphology of Ag-NFIT is intimately related to the pore size and morphology of the AAO membrane**.** The particular pore structure of the CAAO template is responsible for branching of the initially formed Ag-nanowires (Ag-NW), Fig. 1b, while smooth growth is favored in the HAAO template with its smaller and continuous pores, Fig. 1d. The different growth behavior may be rationalized in terms of the expected number of Ag-nuclei per unit area, *N* (that can be obtained from the current-time curve, see supporting information) in comparison to the available nucleation sites, i.e. the number of pores per unit area, *n*. Following the analysis of Zoval et al. *N* should be in the range of $6x10^9$ cm^{-2}, close to *n* for HAAO but larger than *n* of the CAAO membrane.[23] So in the case of HAAO we should expect hemispherical smooth growth of the Ag-NW because the number of Ag-nuclei, *N*, corresponding to the present experimental conditions is smaller than the number of available nucleation sites, whereas in the case of the CAAO membrane the lower number of nucleation sites (in comparison to the expected Ag-nuclei) should lead to a rough morphology and branching of the Ag-NW after nucleation. However, we presume that the large pore size and the branching of the pore channels may also promote growth of the specific NFIT morphology obtained in the case of CAAO. The role of the template in this case should be limited to growth confinement of Ag into the pore channels. In Fig. 2 the XRD patterns show the high degree of preferential <111>-orientation of the Ag-NFIT and Ag-NW, and this independently of their morphology. The hemispherical growth of Ag-NW in the HAAO template should lead to smooth monocrystalline Ag-NW, whereas in CAAO templates epitaxial growth of side branches and particles on the main Ag-NW is expected.

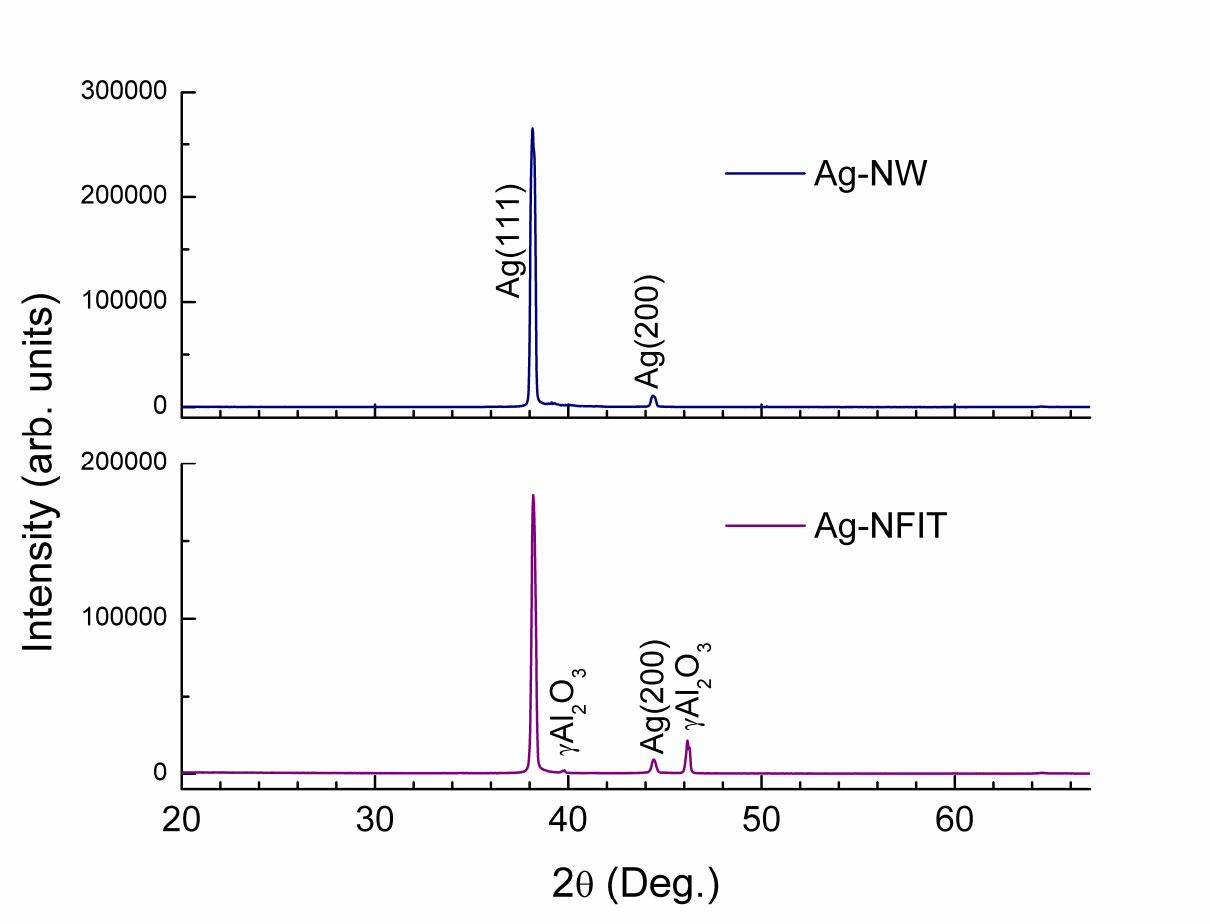

Fig. 2. X-ray diffraction patterns of Ag-NW and Ag-NFIT. Some of residual Al_2O_3 is still detected due to incomplete removal of the CAAO membrane.

SERS investigations were performed on a 10^{-15}M aqueous solutions of rhodamine 6G (R6G) and 10^{-11}M of methyl orange (MO). Figs. 3a and c show the Raman scattering spectra obtained on Ag-NFIT for both R6G and MO, and in comparison to them the spectra obtained with10^{-3}M solutions on an XRD-amorphous Al_2O_3 (processed using sol-gel and spin coating, see experimental section). The main R6G and MO modes are clearly apparent in the spectra with large enhancement on Ag-NFIT. It should be pointed out that the signal enhancement on the Ag-NFIT was reproducible over the whole area of the specimen. The modes are assigned in Figs. 3b for R6G following the description proposed by Hildebrandt and Stockburger.[24] It also appears, following the same authors, that R6G chemisorbs on Ag via its

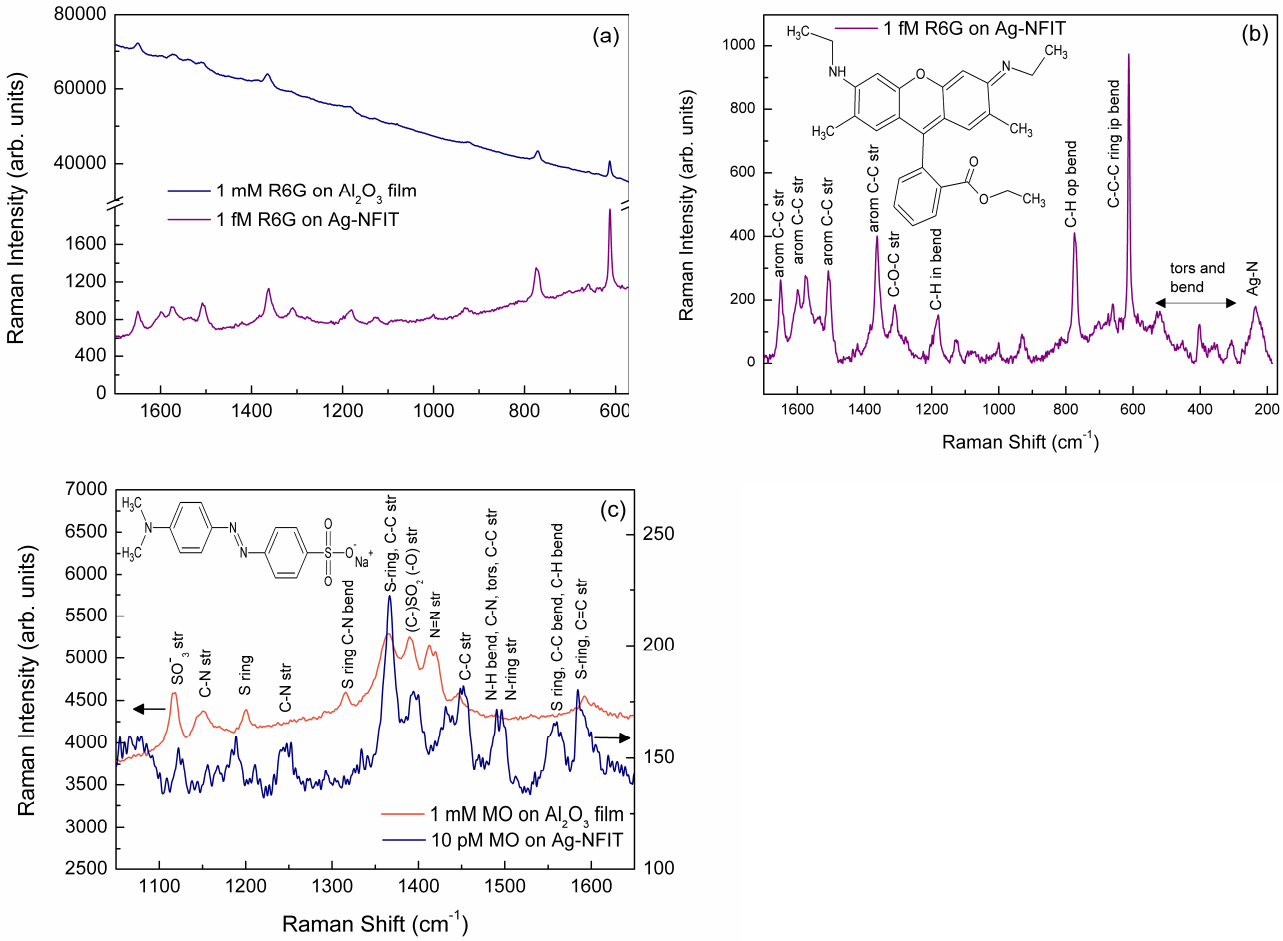

Fig. 3 a) Raman scattering spectra of R6G on a sol-gel Al_2O_3 film (upper patterns) and on Ag-NFIT (lower patterns). The concentration of R6G is 1mM on Al_2O_3 and 1fM on Ag-NFIT. b) Indexing of the different Raman modes of R6G (the inset shows its molecular structure).[24] Note that R6G adsorbs on Ag with its ethylamino-group as indicated by the vibration band at approximately 220 cm^{-1}. c) Raman scattering of MO with a concentration of 1 mM on a sol-gel Al_2O_3 film (upper patterns) and 10pM on Ag-NFIT (lower patterns), with the assignment of the different vibration modes.[25] arom: aromatic; str: stretching; in bend: in-plane bending; op: out-of-plane; tors and bend: torsion and bending modes.

ethylamino-group, forming an Ag-N bond with the stretching vibration mode at approximately 230cm^{-1}.

Comparing the Raman of spectra of MO on Ag-NFIT (SERS) with those of non-SERS (bulk molecules) one notices that the MO lines are differently enhanced and most of them red-shift by approximately 5 to 10 cm^{-1}. This phenomenon was also reported for MO adsorbed on metallic nanowires by Zhang et al..[25] who attributed it to specific interactions between molecule and nanoparticles. The different Raman modes were assigned in Fig. 3c according to Zhang et al.[25] and Machida et al.[26]

The SERS enhancement factors (EF) were calculated from:

$$EF = \left(\frac{I_{SERS}}{C_{SERS}} \frac{C_{RS}}{I_{RS}} \right) \qquad (1),$$

where I_{SERS} is the Raman-band intensity of R6G corresponding to the concentration C_{SERS} on the SERS Substrate, and I_{RS} and C_{RS} the intensity and concentration on non-SERS substrate, respectively. SERS EFs were estimated from different R6G Raman bands as listed in Table 1. The mean SERS EF obtained is approximately $1.2x10^{11}$. In the case of the smooth 70 nm Ag-NWs the SERS EF of $1.6x10^{6}$ obtained was lower by several orders of magnitude, and is in the range of values usually reported for Ag-nanoparticles with comparable particle gap.[16,4] Similarly the SERS EF of MO on Ag-NFIT was calculated taking into account main bands. The mean value of $5x10^{7}$ obtained is largely below that of R6G and should reflect the importance of molecule-metal nanostructure interactions in determining the intensity of the SERS signal.

Wave number of Raman bands of R6G (cm^{-1})	$I_{RS}(10^{-3}M)$	$I_{SERS}(10^{-15}M)x5$	$EFx10^{11}$
1649	3308	1300	0,78
1574	3036	1405	0,92
1506	3057	1455	0,95
1361	3834	2024	1,05
1178	1180	809	1,4
774	3558	2071	1,16
611	4380	4378	2,0

Table 1. Calculation of SERS enhancement factors (EF) for the different R6G Raman bands. I_{SERS} is the Raman-band intensity of R6G corresponding to 10^{-15} M on the SERS Substrate, Ag-NFIT, and I_{RS} the intensity corresponding to 10^{-3} on a sol-gel processed Al_2O_3 film (non-SERS substrate)

Taking into account the concentration of R6G, the analyzed volume and the obtained enhancement factor on Ag-NFIT it is easy to show that Raman signal is from single R6G molecules.[4, 14] The high SERS efficiency of the so processed substrate may be rationalized in the following terms. As pointed out above, SERS enhancement depends strongly on the geometry of the substrate nanostructures for the Raman-active molecules. Loci with strong positive or negative curvature and small gaps in metallic nanostructures provide the hot spots with very large electromagnetic fields, which are required for the large enhancement factors reported for SERS or single molecule SERS. Small gaps and crevices between nanoparticles, or between nanoparticles and more extended structures like wires, have emerged as most promising. The structure presented here is reminiscent of fir twigs, or brushes, and consists of silver nanowires with dense self-assembled short side-branches and particles grown over the length of the nanowire. The branches exhibit a distribution of orientations, lengths, diameters, distances and angles in a way that under the average of the laser spot a distribution of hot spots are acting for signal enhancement. To corroborate the results observed for the present geometry, the electromagnetic fields in the vicinity of the surface were calculated for a simple model structure under laser irradiation. The 3-dimensional simulations were performed with the finite-difference time-domain method for a silver nanowire with two branches, absorbing boundary conditions, and an extended source, using the software package Meep.[29] The field distribution, shown for two perpendicular slices in Fig. 4, exhibits the typical

strong local amplitudes that should account for the high SERS enhancement observed for the Ag-NFIT structure.

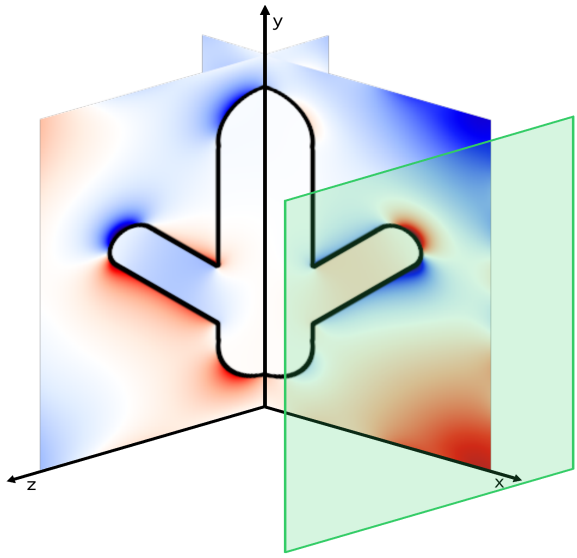

Fig. 4. Snapshot of the electric field propagation simulation along a branched silver nanowire. The *y* component of the electric field along slices in the *x*-*y* and the *y*-*z* planes is shown. Dark colors represent strong fields of positive (red) and negative (blue) orientation. The short silver nanowire (length 140 nm, radius 20 nm) with two branches (length 70 nm, radius 10 nm) along the x and z directions is outlined. The green plane depicts the extended source of a z-polarized field with a wavelength of 532 nm.

4. Conclusions

In conclusion, the results presented in this communication show that particular silver nanostructures can be processed easily using electrodeposition into porous anodic aluminium oxide. Confinement of silver growth into relatively large pore channels produces nanostructures reminiscent of fir twigs with a distribution of sizes, orientation and gaps that act as many hot spots for Raman signal enhancement. With this nanostructure detection of rhodamine 6G and methyl orange could be achieved down to the concentrations of 10^{-15} M (1fM) and 10-^{11}M (10pM), respectively. The

signal enhancement factors of $1.8x10^{11}$ and $5x10^{7}$ obtained should achieve single molecules detection. The main advantages of the proposed SERS substrate are their versatility, reproducibility and cost-effectiveness.

Acknowledgement. Financial funding of this work was provided by the Deutsche Forschungsgemeinschaft (DFG), grant # ES 119/9-1.

References

1 A. Polman, *Science*, 2008, **322**, 868-869.

2 E. Ozbay, *Science*, 2006, **311**, 189-193.

3 W. F. Paxton, S. Sundararajan, T. E. Mallouk and A. Sen, *Angew. Chem. Int. Ed*., 2006, **45**, 5420-5429.

4 S. Nie and S. R. Emory, *Science*, 1997**, 275**, 1102-1106.

5 A. Wei, B. Kim, B. Stadtler and S. L. Tripp, *ChemPhyChem*, 2001, **2**, 743-745.

6 S. Lal, N. K. Grady, J. Kundu, C. S. Levin, J. B. Lassiter and N. J. Halas, *Chem. Soc. Rev.*, 2008, **37**, 898-911.

7 K. L. Wustholz, C. L. Brosseau, F. Casadio and R. P. Van Duyne, *Phys. Chem. Chem. Phys*. 2009, **11**, 7350-7359.

8 C. B. Murray, C. R. Kagan and M. G. Bawendi, *Annu. Rev. Mater. Sci*., 2000, **30**, 545-610.

9 Y. Sun and Y Xia, *Science*, 2002**, 298**, 2176-2179.

10 J. C. Hulteen and C. R. Martin, *J. Mater. Chem*., 1997, **7**, 1075-1087.

11 A. Vlad, M. Mátéfi-Tempfli, S. Faniel, V. Bayot, S. Melinte, L. Piraux and S. Mátéfi-Tempfli, *Nanotechnology*, 2006, **17**, 4873-4876.

12 G. Kartopu, S. Habouti and M. Es-Souni, *Mater. Chem. Phys.*, 2008, **107**, 226-230.

13 Y. Fang, N. H. Seong and D. D. Dlott, *Science*, 2008, **321**, 388-392.

14 A. Campion and P. Kambhampati, *Chem. Soc. Rev.*, 1998, **27**, 241-250.

15 M. Fan and A. G. Brolo, *Phys. Chem. Chem. Phys*. 2009, **11**, 7381-7389.

16 M. Es-Souni, Mar. Es-Souni, S. Habouti, N. Pfeiffer, A. Lahmar, M. Dietze, C-L. Solterbeck, *Adv. Funct. Mater.*, 2009, **20**, 377-385.

17 H. Masuda and K. Fukuda, *Science*, 1995, **268**, 1466-1468.

18 L. Huang, H. Wang, Z. Wang, A. Mitra, K. N. Bozhilov and Y. Yan, *Adv. Mater.*, 2002, **14**, 61-64.

19 G. D. Wei, C-W. Nan, Y. Deng and Y. H. Lin, *Chem. Mater.*, 2003, **15**, 4436-4441.

20 S. Shanmuhk, L. Jones, J. Driskell, Y. Zhao, R. Dluhy and A. R. Tropp, *Nano Lett.* 2006, **6**, 2630-2636.

21 B. Pitrobon, M. McEachran and V. Kitaev, *AcsNano*, 2009, **3**, 21-26

22 A. Tao, F. Kim, C. Hess, J. Goldberger, R. He, Y. Sun, Y. Xia and P. Yang, *Nano Lett.*, 2003, **3**, 1229-1233.

23 J. V. Zoval, R. M. Stiger, P. R. Biernacki and R. M. Penner, *J. Phys. Chem.*, 1996, **100**, 837-844.

24 P. Hildebrandt and M. Stockburger, *J. Phys. Chem.*, 1984, **88**, 5935-5944.

25 A. Zhang, Y. Fang, *chem. Phys.*, 2006, **331**, 55-60.

26 K. Machida, H. Lee, A: Kuwae, *J. Raman spectr.*, 1980, **9**, 1980 198-201.

27 A. F. Oskooi, D. Roundy, M. Ibanescu, P. Bermel, J. D. Joannopoulos and S. G. Johnson, *Computer Physics Communications*, 2010, **181**, 687-702.